Characterization of elastic constants of anisotropic composites in compression using digital image correlation

Olli Orell[a,*], Jyrki Vuorinen[a], Jarno Jokinen[a], Heikki Kettunen[b], Pertti Hytönen[b], Jani Turunen[b], Mikko Kanerva[a]

[a] Department of Materials Science, Tampere University of Technology, P.O. Box 589, FI-33101 Tampere, Finland
[b] Valmet Technologies Oy, P.O.Box 587, FI-40101 Jyväskylä, Finland
*Corresponding author. E-mail address: olli.orell@tut.fi (O.Orell).

ABSTRACT

Experimental determination of elastic constants of anisotropic composite laminates in all orthogonal directions is generally a complex process. In this paper a simple direct technique to determine a broad set of elastic moduli is presented based on compression testing of a prism sample. Digital image correlation is used to measure the full-field deformations that allow the determination of Young's moduli and all six Poisson's ratios for the three orthogonal directions based on a single sample. Finite element model is used in evaluation of the effect of friction on the measured properties. In addition to quantitative characterization of the material properties, local strain mapping is used in qualitative evaluation of the sample structures.

Keywords: laminates, elastic constants, digital image correlation, microstructural analysis

1 INTRODUCTION

To utilize fibre reinforced polymers (FRPs) materials efficiently, it is necessary to have comprehensive knowledge of the material behavior. FRPs are typically transversely isotropic but normally their state of symmetry is orthotropic or in some case fully anisotropic [1,2]. In traditional design of composite structures, the properties of the fabricated materials are routinely estimated and simulated with well-recognized models and theories. Although computer aided calculations are the basis for the design of composites nowadays, experimental testing is still required to confirm the simulations. Also, if the mechanical behavior of a composite structure is to be studied but the exact input data, such as the ply structure or the material properties of the constituents, are unknown, the uncertainty in the simulation results is greatly increased.

Generally, the mechanical testing of FRPs is challenging due to the anisotropic nature, which necessitates numerous tests to be carried out to determine the constants required in describing the mechanical behavior [3,4]. In addition to symmetry-related anisotropy causing orientation-dependent heterogeneity, the microstructure of FRPs is often far from ideal e.g. due to imperfections of manufacturing. These features can cause severe local anomaly differing greatly from the behavior of the global structure. Typically, the tests are carried out using test coupons cut off the laminates fabricated for the purpose. However, it is common for composites that the manufacturing process can have strong influence on the structure, including e.g. reinforcement orientation and volume fraction. In some cases, it can actually be questioned if a simple test coupon correlates with the actual material of the final application or not.

Traditional experimental determination of elastic constants is based on the measured data of the load and the deformations induced in the material. Recently, new indirect determination techniques have also been introduced e.g. based on vibration testing or wave propagation combined with the utilization of genetic algorithms [3,4,5,6,8]. In direct measurements extensometers and electrical resistance strain gauges are routinely used in mechanical testing, and they give averaged strains over the set gauge length. However, the distribution of reinforcements in FRPs is normally in the millimeter range or less [7,9]. If local deformations in composites are to be studied, the spatial resolution of the strain gauges and extensometers is thus not high enough. The anisotropic FRPs call for full-field strain measuring techniques, which include for example Moiré interferometry [10], grating shearography [11], Raman spectroscopy [7], and digital image correlation (DIC) [9,12,13,14]. Especially DIC has recently proven to be efficient technique in the studies of composite structures. In this non-contact measuring technique, strain fields in materials can be studied in conventional manner similar to strain gauges yet simultaneously it allows so called local strain mapping to be carried out offering precise examination of the deformation distribution in a material [7,12,13,15].

Digital image correlation is an optical non-contact method to measure full-field displacements of the studied surface. The technique developed already in 1980’s is well-known and has been described by several authors [12,17,18,19]. In practice, the imaged surface applied with a random speckle pattern is divided into small subsets and the deformations of the surface are computed via algorithms by tracking the spatial shift of the

subsets per image to image. As a result, a complete full-field displacement map of the studied surface is obtained, from which desired deformation analysis can be post-processed. The deformations can even be determined at a sub-pixel accuracy and the measuring frequency depends purely on the performance of the cameras used. While 2D deformations can be measured with one camera, 3D deformations require use of two cameras both of measuring the changes of the deformed surface at different angles.

This work presents a technique to experimentally evaluate a broad set of elastic constants. A similar technique was used earlier by Wang [16] in analysis of properties of anisotropic cartilages. With the technique three Young's moduli and six Poisson's ratios can be determined from a single bulk specimen minimizing thus the need of material quantity. The advantages of the presented technique based on mechanical testing and full-field strain measuring with DIC include: 1) several properties can be determined from a single small test coupon if, for example, only limited amount of material is available, 2) the samples can be made from bulk material fabricated with the identical parameters as the final product and 3) measured off-plane properties of the real component are available. In addition, local strain mapping can be used to examine the micro or macro structure of the extracted samples.

2 EXPERIMENTAL

2.1 Materials and sample preparation

Three different fiber reinforced epoxy laminates fabricated with strip winding technique were studied (Table 1). In addition to these, a single laminate was made with vacuum infusion used in the comparative tests of two different compressive testing techniques. The initial height of the laminates ranged from 8 mm to 12 mm, where the nominal thickness of a fabric ply was 0.5 mm for the wound laminates, and 0.2mm for the vacuum infused laminate. The sample preparation was carried out as follows: 1) cutting of a prism-shaped specimen with edge lengths of 12 mm in laminate 1-2 plane using precision circular saw and 2) grinding of the samples with an in-house built fine mechanical abrasive grinder to achieve highly parallel opposite edges of the prism sample (Fig. 1). The sample height was thus significantly lower than used in the standard compression tests, for example in ASTM D695 (Compressive properties of rigid plastics). However, the two other dimensions were in the same range. The variation in flatness along the sample surfaces was measured to be in the range

of 10-50 µm using optical profilometer (Alicona InfiniteFocus G5). The inclination of the samples was low enough for successful compression testing.

Finally, a random speckle pattern with high contrast was applied on the surfaces of the specimen by spraying with matt alkyd paints. First thin (10-15µm) constant layer of matt white was applied over which black speckles were applied having average diameter of approximately 150µm and thickness of 5-10µm, measured with the optical profilometer.

The reinforcement strip in the material A was aramid fiber mat, and in the materials B and C the strips were uneven-sided woven glass fiber fabrics. The fiber volume fractions were determined using optical microscopy and burn-off technique for the materials containing aramid and glass fibers, respectively. The vacuum infused epoxy laminate (D) consisted of 55 plies of plain weave E-glass fabric.

Table 1. Tested materials. The percentage ratios of reinforcement denote fiber fractions in warp/weft directions.

Sample	Sample size [mm]	Sample height [mm]	Reinforcement (fabric strip)	Matrix	V_f [%]
A	12x12	7	aramid mat	silica-filled epoxy	8
B	12x12	9	glass fabric (52% / 48%)	epoxy	38
C	12x12	10	glass fabric (50% / 50%)	epoxy	29
D	140x12 and 12x12	9	plain glass fabric	epoxy	-

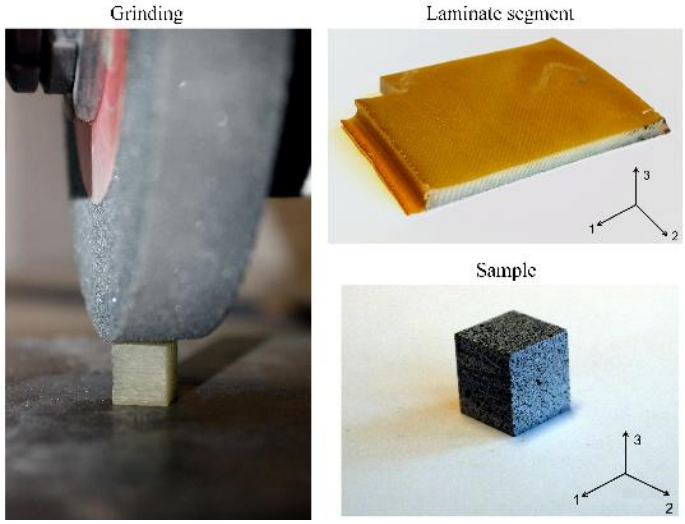

Fig. 1. Specimen preparation and coordinate system, where the strip winding direction is parallel to axis 2.

2.2 Compression testing

Compression testing of the rectangular parallelepiped samples was carried out using a servo-hydraulic universal testing machine (Instron 8800) with a 50kN load cell and manually aligned compression plates with a low surface roughness (Fig. 2a). Self-aligning compression plates with spherical bearing system was tried first but the simultaneous use with DIC was difficult, and smaller manually aligned compression plates were used instead. The alignment was carried out with the help of rotating thin paper between the plates almost at contact, and difference in flatness of less than 30µm across the compression plates could be assumed. The testing rate and the end criteria for each test were set to 0.5 mm/min and 60 MPa, respectively. In each test linear elastic behavior without any significant plastic deformation was presumed, which was ensured by pre-tests. Silicone oil was used between the compression plates and the sample to decrease the effect of lateral friction.

Each sample (n=3) was tested six times in a random order so that for each direction of loading (1-2-3) the deformations were measured from the other two directions as shown in Fig. 3. The tests were denoted by I_{jk}, where *i* is the sample name and indices *j* and *k* are the loading direction and the studied surface normal, respectively.

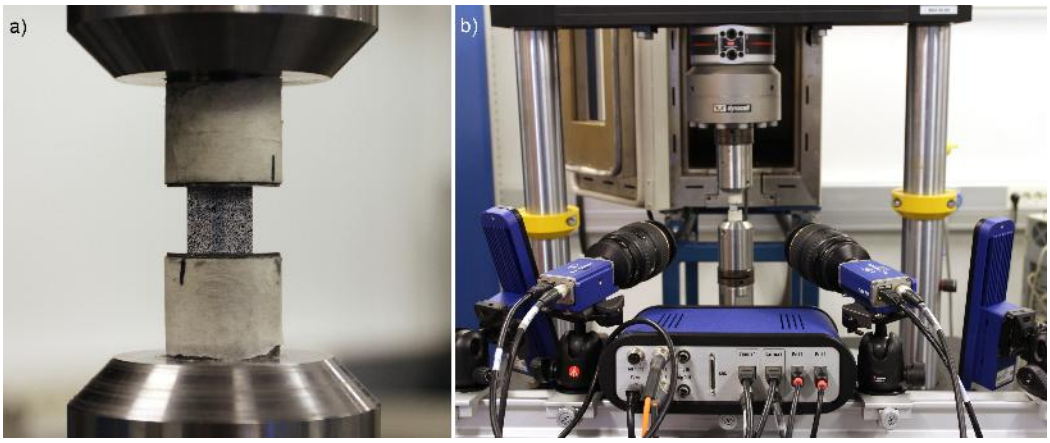

Fig. 2. a) A cubic sample during compression testing **b)** The 3-D DIC test setup

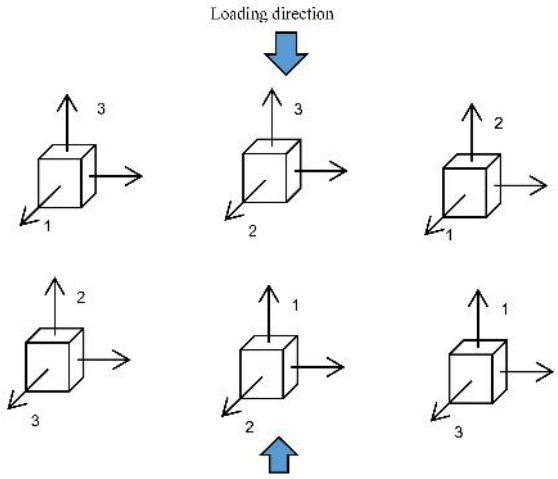

Fig. 3. Test sequence of a prism sample.

In addition to the compression method of the prisms, combined loading compression (CLC) method (ASTM D 6641) was used for comparative testing for single material. The text fixture was compressed with self-aligning compression plates using Instron 5967 universal testing machine with 30 kN load sensor (Fig. 4) The testing rate was 1.3 mm/min and end criteria was 10 kN. The samples cut from the laminate had dimensions of 12 x 9 x 140 mm where the long direction was the direction 1 in the laminate coordination. The gauge length of the unconstrained portion of the sample was thus 13 mm. Before testing electric resistance strain gauges were glued to gauge area: three-axial rosettes (gauge length 5 mm) in the perpendicular surfaces (surfaces 2 and 3) and a single gauge (5 mm) in the opposite side of the surface 3 to detect possible bending of the sample.

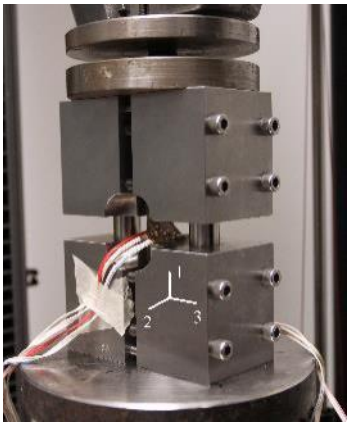

Fig. 4. Combined loading compression test setup

2.3 Digital image correlation analysis

In this study, the deformations were measured with a 3D-DIC system (LaVision) using lenses with a 100 mm focal length and a recording rate of 2 Hz (Fig. 2b). The spatial resolution of the displacement measurement was 15 µm/pixel and the RMS fit of the calibration 0.20 pixel in the first tests with samples A, B and C. In the later tests with material D, the same parameters were 4 µm/pixel and 0.51 pixel. For each measurement, strains were determined both parallel and transverse to loading direction, which enabled the calculation of Poisson's ratios. In addition, the full-field strain maps were used to study local microstructure in the samples.

2.4 Friction measurements

The static and dynamic friction coefficients between the sample and compression plates were determined with CETR UMT-2 tribometer equipped with 200 N 2-D load sensor (Fig. 5). The tests were carried out with and without lubrication to study the effect of greasing on the friction. A prism compression sample with the painted pattern was glued to aluminium pin, which was loaded against the actual compression plate with force 20 N and moved horizontally 4 mm with the velocity of 1 mm/s. The tests were repeated five times from which averages were calculated.

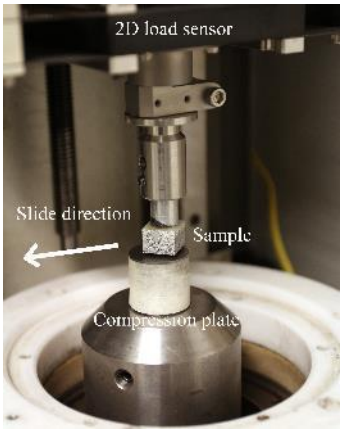

Fig. 5. Measurement of friction coefficients between the coated compression sample and the compression plate.

2.5 Finite element analysis

A finite element model was created for studying the frictional effects. Sample B was chosen as reference, because its properties were expected to be the most oriented. Three-dimensional finite element model was applied using Abaqus/Standard (2016). The model consisted of a ample and two identical rigid parts. The geometry of the sample corresponded sample to the real dimensions (Table 1). The rigid parts were positioned below and above the sample. Surface-to-surface contact was set between the sample and the rigid parts.

Material properties were defined using the Engineering constant option of Abaqus. The option presumes orthotropic relationships. The option applies three Young's moduli, Poisson's ratio (v_{12}, v_{13}, v_{23}) and shear moduli. Young's moduli and Poisson's ratio values were based on experimental results. Shear moduli were approximated based on [26], which provided 3.94 GPa for G_{12} and 4.2 GPa for G_{13} and G_{23}.

Boundary conditions were applied on each part. All translations and rotations of the lower rigid part were restricted. Sample's boundary conditions were applied for restricting the rigid body motion. Horizontal translations were restricted at middle nodal points of the sample upper and lower surface. The sample lower surface edge middle points included restricting boundary conditions parallel to the edge. For the upper rigid part, all translations and rotations excluding vertical translation were restricted. The compression was applied using enforced displacement providing one percent strain in the vertical direction. The sample was meshed using 10,368 solid elements (C3D8). Typical element dimension in the sample was 0.5 mm, which corresponds 18 x 24 x 24 elements for height, width and length, respectively. Rigid parts were meshed using typical 1 mm element dimension. The finite element mesh of the model is shown in Fig. 6.

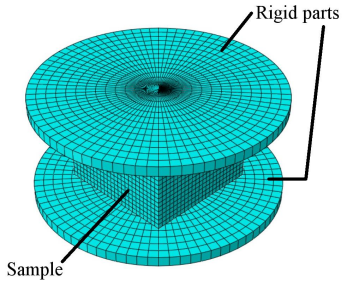

Fig. 6. Finite element model of sample B.

The analyses were performed for three different friction coefficients between the sample and the rigid parts. For comparison, a frictionless analysis was computed. When defining a Poisson's ratio value, average strain in the transverse direction to the loading direction was recorded. The strain was evaluated based on average nodal displacements on the surface of interest. Nodal points closer than 1 mm distance from an edge were not included., since they were not included in DIC analyses. For studying six different Poisson's ratio, the specimen was rotated per analysis according to Fig. 3.

3 RESULTS

Full field strain maps presented in Fig 7 show the local strains in the loading direction. In many cases distributions are very uneven. This arises mainly due to the intrinsic heterogeneous structure of the fiber-reinforced materials but also due to the lack of perfect parallelism between the contact surfaces causing deviation from a truly uniaxial loading condition. Even though DIC is a fuzzy measuring technique [20] in which average displacements are computed over defined subsets, the spatial resolution of full-field measurements is usually excellent compared to conventional strain measurement techniques. However, there are certain limitations when studying local deformations in heterogeneous materials since the subset size should be smaller than the size of the heterogeneity [20,21]. If there are different materials inside a subset, the averaging process leads to blurred measuring artefacts at the interface regions, which is a fundamental effect of the technique. In a DIC measurement, there are several factors affecting the outcome of the analysis (such as speckle pattern size, subset size and used magnification). Compromises have to be made to obtain large enough study window, sufficient spatial resolution and low noise.

In this study, with the first tests (materials A, B and C) the DIC analysis was given a subset size of 21 pixels with a 5-pixel step size. In the latter test with material D the parameters were 39 pixels and 10 pixel, respectively. These parameters have a strong influence on the computed strain fields, as explained in [22,23]. Different subset and step sizes were studied and the selected parameters presented a good combination of low noise and good spatial resolution of the local strain fields in the measurements.

Engineering constants (i.e. E, ν, G) in macroscale are generally used to define mechanical behavior of FRPs, which simplifies for example the design process of a component and the comparison with conventional monolithic materials. In that case the local material characteristics are disregarded and the structures are treated as a homogeneous continuum with, for example, orthotropic material properties [3]. In this study, the strains were determined over the whole analyzed surface, excluding 1 mm edge borders thus giving a representative mean values for the measured quantities.

3.1 Microstructural observations with local strain mapping

Due to the inhomogeneous microstructure consisting of the reinforcement fiber bundles in polymer matrix, great deformation concentrations and strain gradients are formed in the composite materials under stress. In Fig. 7 three optical microscope images are shown for the different polished surfaces of the studied materials (B and C), where the distribution of the glass fiber bundles is clearly visible in the cross sections. The right column of the figure shows the axial strains under compression measured with DIC from the same surfaces. By combining the optical and DIC images a concrete indication of the spatial resolution of the measured strain can be seen. It is seen that the high strain areas under compressive stress locate precisely at the matrix regions in the studied flat surfaces whereas remarkably lower strains are observed at the roving locations, where the reinforcement volume fraction is locally high. In addition to the reinforcement yarn distribution at the studied surface, surface and sub-surface voids can be detected from the full-field strain maps seen as locally increased strain spots shown in Fig. 7b.

Fig. 8a shows the line plot of the axial through-thickness strains (in direction 3) shown in Fig. 7f. The average strain over the studied surface is -0.8 % but locally the strain fluctuates between -0.3 % at the reinforcements and -1.5 % at the matrix rich locations. The decreasing strain from top to bottom of the studied surface can be explained by the reinforcement content gradient at the cut surface. This can arise either due to uneven actual reinforcement distribution in the material or by the small variation in the location of separate plies in through-thickness direction at the cut surface.

The small fluctuations in the axial strain arise from the alternating reinforcement and matrix components of the multilayer laminate at the cross section, from which the ply count of the laminate can be calculated. It should be noticed that whereas the optical image shows the reinforcement distribution only at the cut surface, the deformations under loading at the free surface measured with DIC are partly affected by properties of the material below the studied surface.

Fig. 8b shows the local strains from the diagonal line shown in Fig. 7i which is the in-plane surface of the thick laminate. Here the axial strain fluctuates between -0.3% and -1.8% and the mean strain in the surface is -0.7%. The minimum compressive strain is found in the middle of the warp yarn whereas the maximum

compressive strain is located at the resin pockets which form over the space between warp and weft yarns of the fabric.

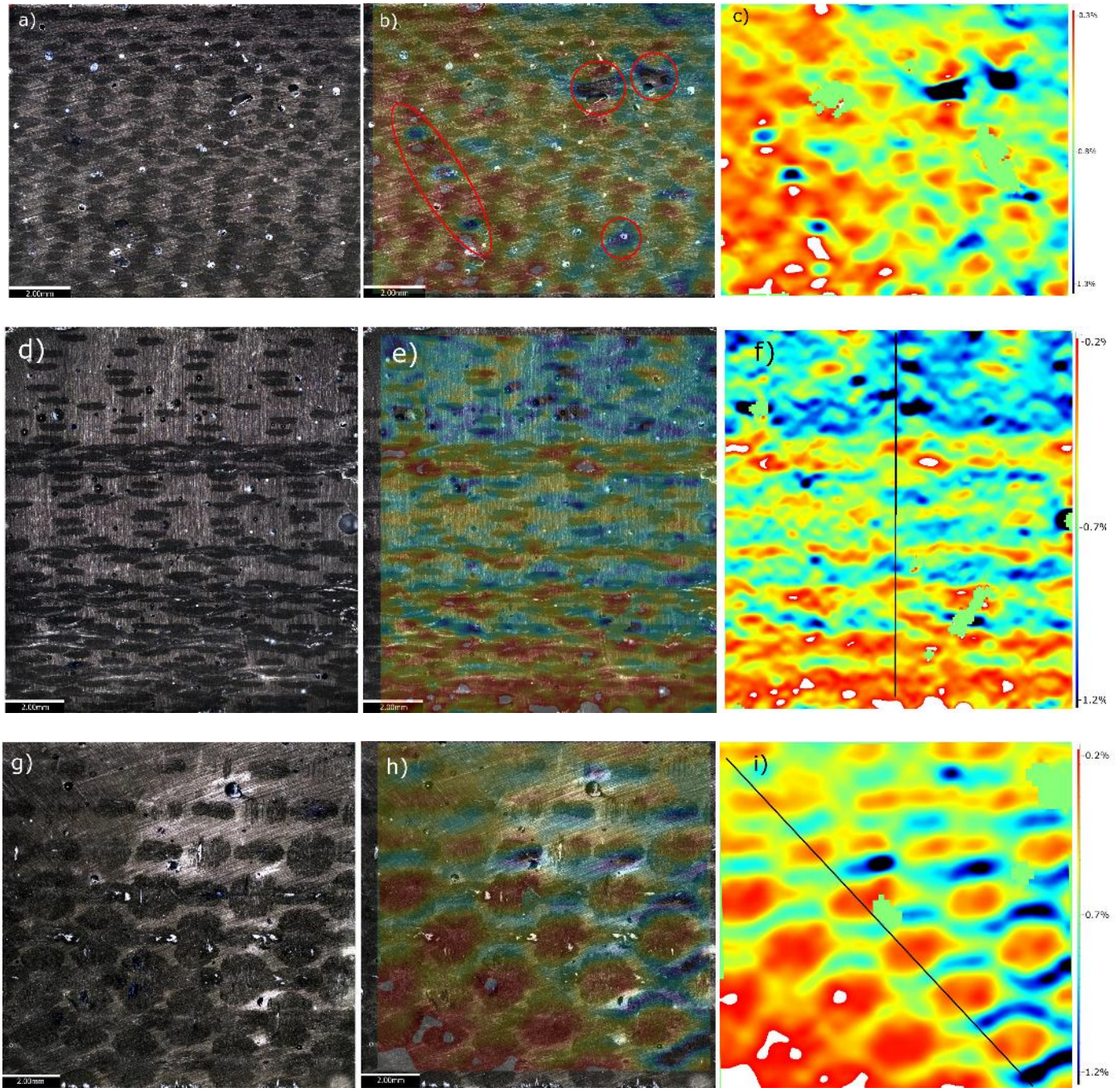

Fig 7. Left column = optical microscopy, Middle column = pseudo image, Right column = axial strain from DIC measurements. Top row = material B, surface 2; Middle row = material C, surface 1; Bottom row = material B, surface 3.

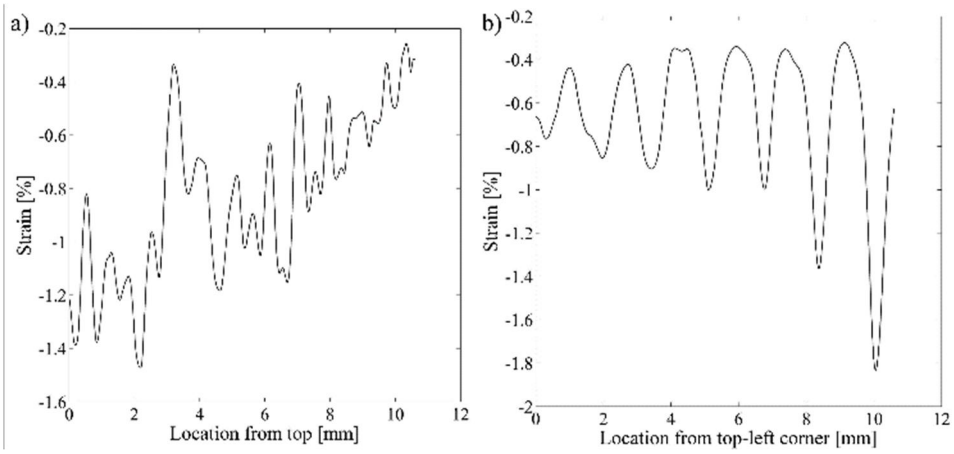

Fig. 8. Axial strain along **a)** the vertical line in Fig. 5f and **b)** the diagonal line in Fig. 5i

3.2 Elastic moduli

Elastic moduli of the samples were calculated as a secant modulus from the initial part (appr. $\Delta\varepsilon$=0.0005…0.003) of the stress-strain curve based on compressive load. An example of the axial strain map at 50 MPa compressive stress and a stress-strain curve for the material are shown in Fig. 9. The curves show no significant plastic deformation confirming the initial assumption that no remarkable irreversible deformation occurs in the samples, which could affect detrimentally the results when the same sample is tested six times.

The measured moduli for each tested material are shown in Fig 10 and Table 2. The slightly higher E_2 compared to E_1 can be explained with the higher crimp in the fabrics in transverse direction compared to winding direction causing increased off-axis orientation of the reinforcement in direction 1. In addition, the fiber content in material B (52% / 48%) was higher in direction 2 increasing the modulus. The high E_3 of material A in terms of its low fiber content is due to the high inorganic filler content of the resin.

Table 2. Determined engineering elastic constants for the materials A, B and C.

	E_1 [GPa]	E_2 [GPa]	E_3 [GPa]	ν_{12}	ν_{21}	ν_{13}	ν_{31}	ν_{23}	ν_{32}
A	6.8	7.0	6.5	0.34	0.36	0.4	0.38	0.40	0.30
B	15.3	16.8	7.4	0.25	0.19	0.48	0.22	0.46	0.21
C	10.4	11.3	6.1	0.27	0.22	0.48	0.27	0.42	0.23

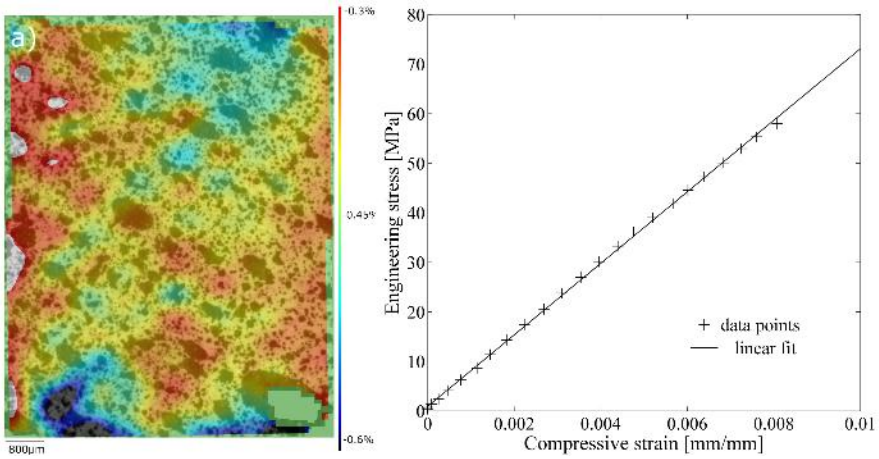

Fig. 9. a) Full-field strain map of the test B_{21} showing compressive strain in direction 2 (vertical in the figure), P = 50 MPa. **b)** Apparent stress-strain curve of the test B_{21}.

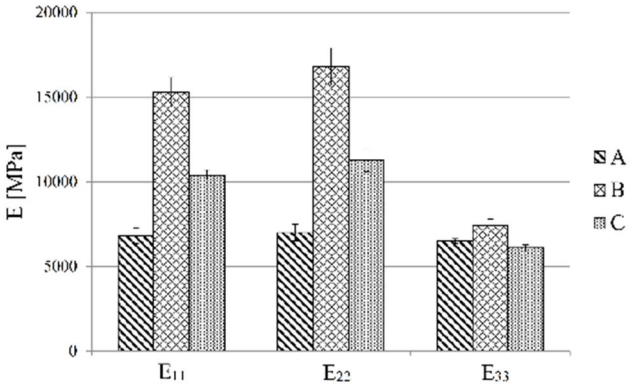

Fig. 10. Determined apparent Young's moduli of the materials.

3.3 Poisson's ratios

Precise determination of Poisson's ratios of materials is generally challenging: 1) it requires simultaneous measurements of strain in two accurately perpendicular directions, 2) the percentage errors in transverse strain measurements can be large and 3) uniaxial stress state is required. Since the transverse strains are usually lower than the axial strains, Poisson's ratios are normally calculated over a higher strain region than what is used for modulus determination, as recommended, for example by ISO-527 for tensile tests [24]. The strains are usually measured with extensometers or biaxial strain gauges, with whom the misalignment of the measuring devices can have a significant effect on the results. On the other hand, with DIC there are several different factors which can have an effect on the measured strains, such as the quality of the calibration, the used surface pattern and the chosen analysis parameters (subset size, step size, etc.). However, from the full

field strain data obtained with 3D-DIC analysis Poisson's ratios can be rather practically determined over the studied surface provided that the strains are high enough considering the resolution of the measurement.

Here, the Poisson's ratios (ν_{yx}) were calculated for each loading orientation as a ratio of transverse strain in the x-direction (transverse to load direction) and axial strain in the y-direction (load direction). Generally, the full-field figures (e.g. Fig. 11a) showed very uneven values of Poisson ratio on the studied surfaces, which is explained by the actual inhomogeneous microstructure of the composite, i.e. caused by the distribution of the fibre bundles in the woven reinforcements. However, when a mean value is calculated over the data, a representative apparent homogenous property can be obtained. In Fig. 11b the apparent ν_{32} of material C is plotted against the axial strain. With the lowest strain values ν_{32} fluctuated presumably due to uneven loading conditions of the samples with the compression plates and the very small transverse strains considering the resolution of the technique. At higher axial strains, the ratio stabilizes and an average value of the Poisson's ratio was determined from the axial strain range of (0.003…0.006). Results of the six Poisson's ratios for the three materials are shown in Fig. 12.

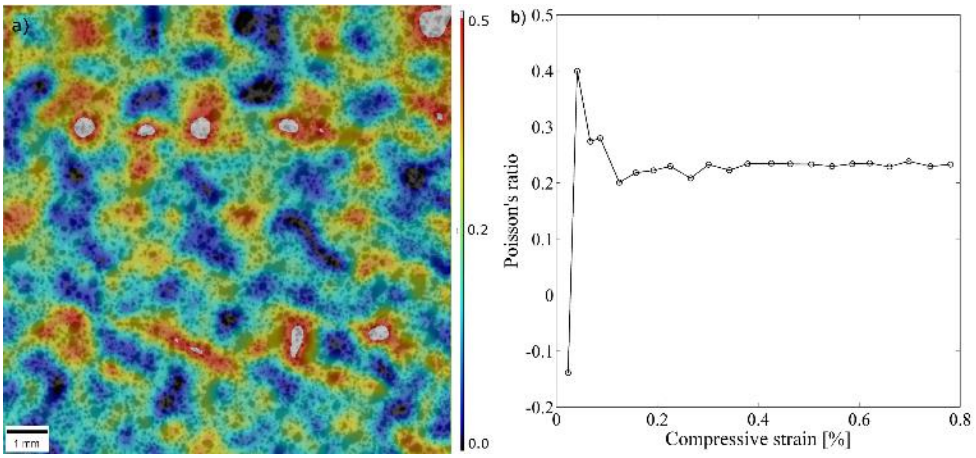

Fig. 11. a) Full-field map for ν_{32} of material C, P = 50 MPa. **b)** Areal mean value of ν_{32} as a function of strain measured.

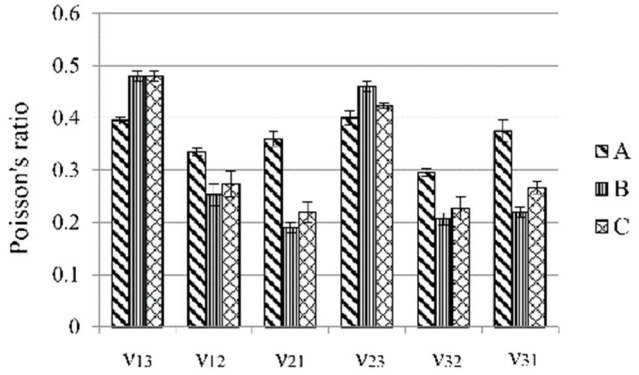

Fig. 12. Determined Poisson's ratios of the materials.

3.4 Friction effects

The FEM simulations indicated that the friction between the sample and the compression plates had insignificant effect on the deformation in the loading direction. Thus, the experimentally determined Young's moduli can be considered valid. However, the friction restraining the lateral deformations of the sample at the contact plane has an effect on the Poisson's ratio as shown in Fig. 13. The higher the friction coefficient, the greater the effect (that decreases Poisson's ratio values) on the Poisson's ratios, which gives reasons to use polished and lubricated compression plates in the compression tests.

Actual friction coefficients were determined using real contact surfaces used in the compression tests. On the dry plate the composite sample with the sprayed pattern showed static and dynamic friction coefficients of 0.23 and 0.18, respectively. By lubricating the compression plate with silicone oil the friction coefficients decreased to 0.14 and 0.09, respectively (Fig. 14). Due to the friction effect the measured Poisson's ratios in these tests are thus approximately 3 % - 7% lower than for compression with zero friction.

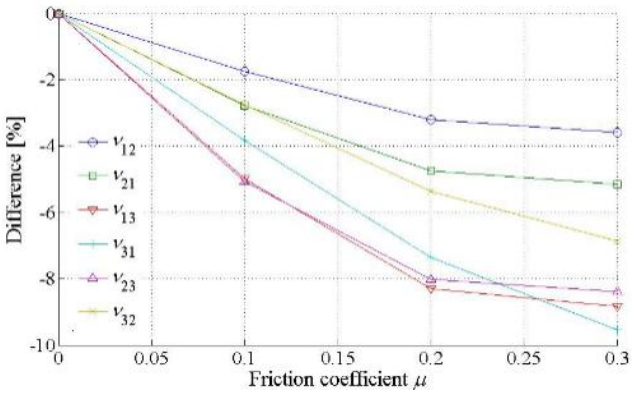

Fig 13. Simulated effect of the friction between compression plates and sample on Poisson's ratios for sample B.

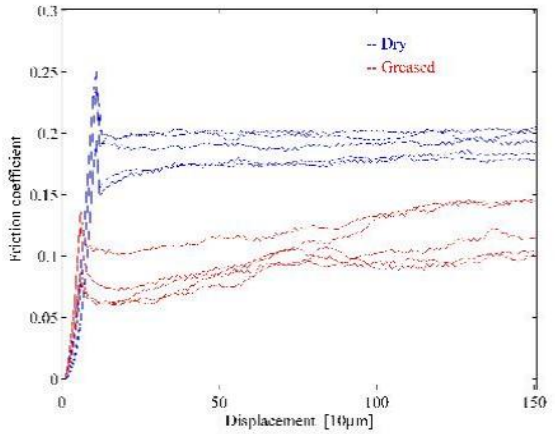

Fig. 14. Measured friction coefficients of the painted compression prism sample against dry and greased compression plate

3.5 Comparison of the compression methods

To evaluate the robustness and accuracy of the prism compression technique, five samples (140 mm x 12 mm x 9 mm) from laminate D were tested with the combined loading compression method (according to ASTM D 6641) to determine Young's moduli E_1 and Poisson's ratios ν_{12} and ν_{13}. After that, the compression tests using DIC and prism samples (12 mm x 12 mm x 9 mm) made of the same laminate were carried out to determine the same properties.

The results presented in Table 3 show that both methods give good correspondence for modulus E_1, indicating that the axial strain determinations are consistent. The measured Poisson's ratios, on the other hand, show significant difference where the trend is that the combined loading compression gives lower values (-18% and -20 %). The higher standard deviation in the values measured with DIC is due to lower strain resolution compared to strain gauges, which is emphasized with the transverse strains being significantly lower.

However, the observed difference in Poisson's ratios can largely be explained with the different boundary conditions of the samples in the test methods. In the combined loading compression method the sample is fully constrained in direction 3, and likely also in the direction 2 because the friction between the sample and text fixture is high on purpose. In the prism compression test, on the contrary, the lateral constrains are remarkably lower, in which the friction coefficient was shown to be approximately 0.15. The greater the lateral constrains in the gauge ends the lower the Poisson's strains are during the compression.

Table 3. Measured properties for the laminate D with two different test methods. (n=5, average values and their standard deviation)

Test	Studied surface	E_1 [GPa]	ν_{12}	ν_{13}
ASTM D 6641 with strain gauges	S2	20.4 (2.8)		0.393 (0.005)
ASTM D 6641 with strain gauges	S3	25.9 (1.9)	0.163 (0.004)	
Prism compression with DIC	S2	21.7 (1.7)		0.476 (0.014)
Prism compression with DIC	S3	26.6 (2.0)	0.205 (0.020)	

4 DISCUSSION

4.1 Sample size and edge effects

In the determination of apparent mechanical properties of anisotropic materials using small samples the question of adequate sample size is of essential importance. Through-thickness properties, especially through-thickness strength, have been determined with parallel-sided prism samples similar to used in this study by several research groups. [28-32] In the studies typical sample edge length has been 10 mm – 12 mm, and it has been shown that the compressive stress below the contact plane becomes stable normally after the distance of approximately 10% of their total thickness [30,31].

Although the stress distribution in sample under compression is dependent on the properties of the reinforcement, stacking sequence and global orientation of the sample, in terms of the constant stress state required for successful measurements, the size of the prism samples used in our tests was deemed suitable for testing.

In addition to the stress concentrations close to the compression plates, in laminates adjacent to free edges there exists a narrow region in which large interlaminar normal and shear stresses exist. Several authors [29,33] have commented that the prism specimens are subjected to these free-edge effects but their impact on the measured properties is seldom analysed in detail. With a comprehensive FE analysis Thompson showed that the edge-effects can be remarkable, but were almost fully dissipated after 1.5 mm from each edge (12 mm) into the centre of sample. [31]

The edge effects are thus always present in laminated materials, which can have an effect on the experimentally measured strains on the free surfaces causing, for example, inaccuracy in the determined modulus values.

When compared the determined elastic properties of the same material measured with the two different compression techniques (Table 3), it is observed that the both give statistically similar values for E_1. However, the modulus determined with the surfaces normal to axis 2 and 3 differed significantly, on the contrary to the initial assumption. The difference is presumed to be affected by the two different phenomena. Firstly, the edge effects in the surface 2 are greater than in the surface normal to laminate thickness (surface 3). Secondly, even though the volume fraction of the reinforcement in the small sample is more or less constant, the relative area of the reinforcement in the ground surfaces can differ between the edges of the prism. The strains are measured purely from the surface and, for example, in Fig. 7 it is seen that locally the strains fluctuate significantly over the studied surface. This phenomenon is emphasized when woven reinforcements with larger repeating units are used. Kim et al suggested that the minimum edge length of a sample should be at least twice of the repeating unit with at least one repeating unit in order that the sample can be considered to be a representative sample from the structure [29]. When determining strains from the surface, similar assumption can be made, i.e. the gauge length in strain measurement (in the middle area where the compression stress state is not affected by the loaded ends) should at least twice the length of repeating unit of the reinforcement giving a rough guideline for the minimum dimensions of the sample.

4.2 Anisotropy

In essence, the properties of anisotropic materials are dependent on the direction of the material. The elastic behavior of fully anisotropic materials can be described with 21 independent elastic constants. With

continuous fibre reinforced composites, often some planes of symmetry exist, which reduces the number of the individual elastic constants. FRPs are typically orthotropic, thus, have three mutually orthogonal planes of symmetry reducing the number of the individual constants to nine [1,2].

For linear orthotropic materials, only three Young's moduli and three Poisson's ratios are independent. Thus, the Poisson's ratios and Young's moduli are coupled with the following relationship:

$$\frac{\nu_{ij}}{E_i} = \frac{\nu_{ji}}{E_j} \leftrightarrow \frac{\nu_{ij}}{\nu_{ji}} = \frac{E_i}{E_j} \qquad (1)$$

Fig. 15a shows the $\frac{\nu_{ij}}{\nu_{ji}}$ vs $\frac{E_i}{E_j}$ –plot, where the three determined moduli ratios based on the DIC measured values of each material are plotted together with an orthotropic model (the diagonal line). The coupled moduli ratios of material A match amidst point (1,1), indicating that the properties were only slightly dependent on the orientation. The materials B and C, in contrast, show greatly scattered moduli ratios explained by increased anisotropy due to the fabric reinforcements.

The fiber content in the warp and weft directions of the reinforcements used in materials B and C were 52/48 and 50/50, respectively. However, the determined E_1 and E_2 of materials B and C were observed to differ significantly based on Student's t-test ($p<0.05$) for both materials. The weaving pattern of the reinforcements was uneven-sided, and different in the tested materials. Moreover, during manufacturing the fabric strips are tensioned slightly in the direction 2 causing straightening of the fibers. Thus, the difference in the moduli is considered to result mostly due to the different level of undulation of fibers in the two directions.

The percentage coupling difference (Δ) between theoretical and measured elastic moduli can be calculated by

$$\Delta_{ij} = 100 \times \left(1 - \frac{\frac{\nu_{ij}}{\nu_{ji}}}{\frac{E_i}{E_j}}\right) \qquad (2)$$

where *i* and *j* denote the orthogonal directions 1, 2 and 3. The calculated coupling differences for the materials B and C are presented in Fig. 15b, where it is seen that especially Δ_{12} is significant. It is well known that the tensile and compressive moduli of fiber reinforced materials are different, mainly due to the local

microbuckling or kinking phenomena of fibers under compression decreasing the compressive modulus [27]. In the compression tests, the axial loading causes compression whereas, due to the Poisson's effect, tensile stresses are generated in the transverse directions. The difference between E_t and E_c, is presumably taking also part, in addition to the edge-effects, into the observed variation of measured values and the theoretical symmetrical elastic behavior, explained by Eq. 1.

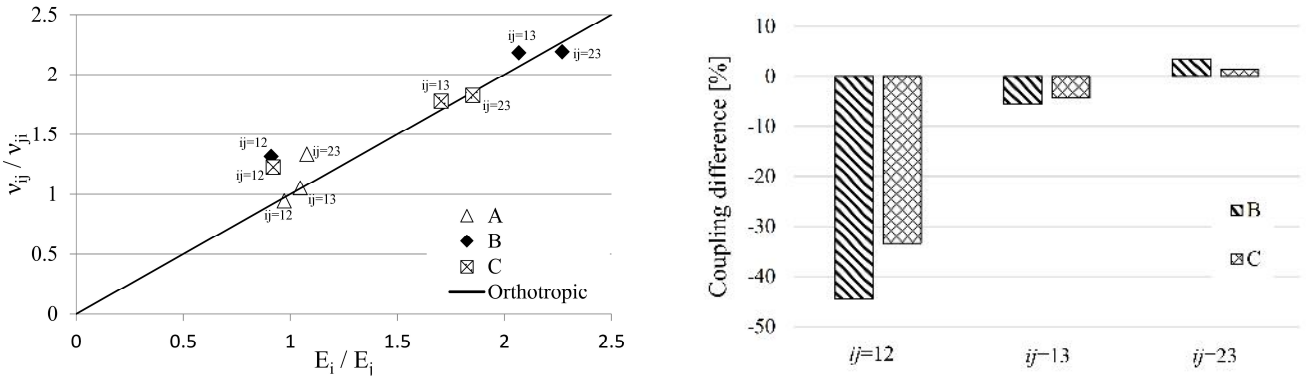

Fig. 15. a) Evaluation of the elastic behavior of the materials (i, j = from 1 to 3). b) Difference between theoretical and measured coupling of Poisson's ratios and Young's moduli.

5 CONCLUSIONS

Digital image correlation is an effective non-contact full-field technique to study surface deformations. In this research we used DIC to determine deformations of cubic samples made of thick polymer composite laminates under compression. By measuring a sample in six different test orientations nine engineering elastic constants, i.e. three Young's modulus and six Poisson's ratios, were determined directly based on the single sample for three different composite materials. The properties are generally arduous to measure and also difficult to simulate, because the out-of-plane properties of the multilayer fabric reinforced composites are often unknown.

For successful compression testing, highly parallel opposite edges of the rectangular cubic sample are required, which complicates the sample manufacturing. However, with the presented technique, the required

amount of sample material is at a minimum. This allows a broad set of elastic material properties in three orthogonal directions to be directly determined, for example, from a piece of material used in a real application. This is a clear benefit if, for example, the microstructure of a composite component is strongly dependent on the fabrication technique, and the manufacturing of conventional test coupons with the same technique is challenging or impossible. A rule of thumb of two repeating units can be used for the absolute minimum edge length for the compression sample. Here, a sample edge length of 12 mm was used.

The measured compressive Young's moduli showed reasonable agreement when considering the microstructure of the materials. The measured elastic moduli were analyzed against an orthotropic material model and the results showed good correspondence with the model. The actual friction coefficients between the tested samples and the compression plates were measured. The effect of friction on the measured properties was analyzed with a finite element model, which indicated that, on the measured Young's moduli, the effect is minimal but resulting in lower values of the Poisson's ratios. The comparison of the Young's moduli and Poisson's ratios in single loading direction measured with the prism compression technique and ASTM D6641 standard test was carried out. The determined Young's moduli were in a good agreement but the Poisson's ratios measured with ASTM D6641 showed lower values. The difference was largely explained with the differences in the constraints between the tests.

In addition to the quantitative determination of the engineering moduli, the full-field strain measuring technique with very good spatial resolution allows local strain mapping of the samples. This can be used in evaluation of the microstructure (e.g. reinforcement distribution, local defects) of the materials, but also to ascertain that the strains are measured from a representative location on the sample surface.

Acknowledgements

The work has been done as a part of the FIMECC Hybrids research program supported by the Tekes - Finnish Funding Agency for Technology and Innovation and the participating companies. The authors would like to thank Tekes for the financial support and Mr. Mika Pihlajamäki and Mr. Tommi Lehtinen for helping with the experiments.

REFERENCES

[1] Hull D, Clyne TW. An introduction to composite materials. Cambridge Solid State Science Series, 1981.
[2] Reddy JN. Mechanics of laminated composite plates and shells: Theory and analysis. CRC press LLC, 2004
[3] Lasn K, Klauson A, Chati F, Décultot D. Experimental determination of elastic constants of an orthotropic composite plate by using lamb waves. Mech Compos Mater 2011;47(4):435-446
[4] Lasn K, Echtermeyer AT, Klauson A, Chati F, Décultot D. Comparison of laminate stiffness as measured by three experimental methods. Polym Test 2015;44:143-152.
[5] Vishnuvardhan J, Krishnamurthy CV, Balasubramaniam K. Genetic algorithm reconstruction of orthotropic composite plate elastic constants from a single non-symmetric plane ultrasonic velocity data. Compos Part B 2007;38(2):216-227.
[6] Kersemans M, Paepegem WV, Abeele KWD, Pyl L, Zastavnik F, Sol H, Degrieck J. The Quasi-harmonic ultrasonic polar scan for material characterization: Experiment and numerical modeling. The 12th International Conference of the Slovenian Society for Non-Destructive Testing, September, 2013.
[7] Potluri P, Young RJ, Rashed K, Manan A, Shyng YT. Meso-scale strain mapping in UD woven composites, Compos Part A:Appl Sci Manuf 2009;40(12):1838-1845.
[8] Vuorinen JE, Schwarz RB, McCullouh C. Elastic constants of an aluminum-alumina unidirectional composite. J Acoust Soc Am 2000;108(2):574-579.
[9] Anzelotti G, Nicoletto G, Riva E. Mesomechanic strain analysis of twill-weave composite lamina under unidirectional in-plane tension, Compos Part A 2008;39(8):1294-1301.
[10] Kadooka K, Kunoo K, Uda N, Ono K, Nagayasu T. Strain analysis for Moiré interferometry using the two-dimensional continuoso wavelet transform. Exp Mech 2003;43(1):45-51.
[11] Lee JR, Molimard J, Vautrin A, Surrel Y. Digital phase-shifting grating shearography for experimental analysis of fabric composites under tension. Compos Part A 2004;35(7-8):849-859.
[12] Ivanov D, Ivanov S, Lomov S, Verpoest I. Strain mapping analysis of textile composites, Opt Lasers Eng 2009;47(3-4):360-370.
[13] Daggumati S, Voet E, Paepegem WVV, Degrieck J, Xu J, Lomov SV, Verpoest I. Local strain in a 5-harness satin weave composite under static tension: Part I – Experimental analysis. Compos Sci Technol 2011;71(8):1171-1179.
[14] Flament C, Salvia M, Berthel B, Crosland G. Local strain and damage measurements on a composite with digital image correlation and acoustic emission. J Compos Mat 2016;50(4):1989-1996.
[15] Daggumati S, In-situ local strain measurement in textile composites with embedded optical fibre sensors. 5th International conference on Emerging Technologies in Non Destructive Testing (ETNDT-5), 2011.
[16] Wang CC, Chahine NO, Hung CT, Ateshian GA. Optical determination of anisotropic material properties of bovine articular cartilage in compression. J Biomech 2003;36(3):339-353.
[17] Heinz SR, Wiggins JS. Uniaxial compression analysis of glassy polymer networks using digital image correlation, Polym Test 2010;29(8):925-932.
[18] Sánchez-Arévalo FM, Pulos G. Use of digital image correlation to determine the mechanical behavior of materials. Mater Charac 2008;59(11):1572-1579.
[19] Jerabek M, Major Z, Lang RW. Strain determination of polymeric materials using digital image correlation. Polym Test 2010;29(3):407-416.
[20] Canal LP, González C, Molina-Aldarequía JM, Segurado J, Llorca J. Application of digital image correlation at the microscale in fiber-reinforced composites. Compos Part A 2012;43(10):1630-1638.
[21] Rajan VP, Rossol MN, Zok FW. Optimization of digital image correlation for high-resolution strain mapping of ceramic composites. Exp Mech 2012;52(9):1407-1421.
[22] Rossi M, Lava P, Pierron F, Debruyne D, Sasso M. Effect of DIC spatial resolution, noise and interpolation error on identification results with the VFM. Strain 2015;51(3):206-222.
[23] Wang Y, Lava P, Coppieters S, De Strycker M, Van Houtte P, Debruyne D. Investigation of the uncertainty of DIC under heterogeneous strain states with numerical tests. Strain 2012;48(6):453-462.
[24] ISO-527-1:2012, Plastics – Determination of tensile properties
[25] Lempriere BM. Poisson's ratio in orthotropic materials, AIAA Journal 1968;6(11):2226-2227.

[26] Naik NK, Chandra Sekher Y, Meduri S. Damage in woven-fabric composites subjected to low-velocity impact, Compos Sci Technol 2000;60:731-744
[27] Meng M, Le HR, Rizvi MJ, Grove SM. The effects of unequal compressive/tensile moduli of composites, Compos Struct 2015; 126:207-215
[28] Tagarielli VL, Minisgallo G, McMillan AJ, Petrinic N. The response of a multi-directional composite laminate to through-thickness loading, Compos Sci Technol 2010; 70:1950-1957
[29] Kim BC, Park DC, KIM BJ, Lee DG. Through-thickness compressive strength of a carbon/epoxy composite laminate, Compos Struct 2010; 92:480-487
[30] Lee DG, Park DC. Through-thickness compressive strength of carbon-phenolic woven composites, Compos Struct 2005; 70:403-412
[31] Thompson LF. Through-thickness compression testing and theory of carbon fibre composite materials, PhD Thesis 2011, School of Mechanical, Aerospace and Civil Engineering; University of Manchester
[32] Guo Y, Post D, Han B. An experimental study of micromechanical behavior and smeared engineering properties, J Compos Mat 1992; 26(13):1930-1944
[33] Mespoulet S, Hodgkinson JM, Matthews FL, Hitchings D, Robinson P. Design, development, and implementation of test methods for determination of through thickness properties of laminated composites, Plast Rub Comp 2000;29(9):496-502

Figure captions

Fig. 1. Specimen preparation and coordinate system, where the strip winding direction is parallel to axis 2.

Fig. 2. a) A cubic sample during compression testing **b)** The 3-D DIC test setup

Fig. 3. Test sequence of a prism sample.

Fig. 4. Combined loading compression test setup

Fig. 5. Measurement of friction coefficients between the coated compression sample and the compression plate.

Fig. 6. Finite element model of sample B.

Fig 7. Left column = optical microscopy, Middle column = pseudo image, Right column = axial strain from DIC measurements. Top row = material B, surface 2; Middle row = material C, surface 1; Bottom row = material B, surface 3.

Fig. 8. Axial strain along **a)** the vertical line in Fig. 5f and **b)** the diagonal line in Fig. 5i

Fig. 9. a) Full-field strain map of the test B_{21} showing compressive strain in direction 2 (vertical in the figure), P = 50 MPa. **b)** Apparent stress-strain curve of the test B_{21}.

Fig. 10. Determined apparent Young's moduli of the materials.

Fig. 11. a) Full-field map for ν_{32} of material C, P = 50 MPa. **b)** Areal mean value of ν_{32} as a function of strain measured.

Fig. 12. Determined Poisson's ratios of the materials.

Fig. 13. Simulated effect of the friction between compression plates and sample on Poisson's ratios for sample B.

Fig. 14. Measured friction coefficients of the painted compression prism sample against dry and greased compression plate

Fig. 15. a) Evaluation of the elastic behavior of the materials (i, j = from 1 to 3). b) Difference between theoretical and measured coupling of Poisson's ratios and Young's moduli.